In vivo endoscopic tissue diagnostics based on spectroscopic absorption, scattering, and phase function properties

Philippe Thueler
Swiss Federal Institute of Technology
Applied Optics Institute
PO Box 127
CH-1015 Lausanne
Switzerland
E-mail: philippe.thueler@bigfoot.com

Igor Charvet
University of Geneva
School of Medicine
Department of Morphology
Rue Michel Servet 1
CH-1211 Geneva 4
Switzerland

Frederic Bevilacqua
Swiss Federal Institute of Technology
Applied Optics Institute
PO Box 127
CH-1015 Lausanne
Switzerland
    and
University of California, Irvine
Beckman Laser Institute
Laser Microbeam and Medical Program
1002 Health Sciences Road East
Irvine, California 92612

M. St. Ghislain
Swiss Federal Institute of Technology
Applied Optics Institute
PO Box 127
CH-1015 Lausanne
Switzerland

G. Ory
Geneva University Hospital
Internal Medicine Department
Rue Micheli-du-Crest 24
CH-1205 Geneva
Switzerland

Pierre Marquet
University of Lausanne
Institute of Physiology
R. Bugnon 7
CH-1005 Lausanne
Switzerland

Paolo Meda
University of Geneva
School of Medicine
Department of Morphology
Rue Michel Servet 1
CH-1211 Geneva 4
Switzerland

Ben Vermeulen
Geneva University Hospital
Internal Medicine Department
Rue Micheli-du-Crest 24
CH-1205 Geneva
Switzerland

Christian Depeursinge
Swiss Federal Institute of Technology
Applied Optics Institute
PO Box 127
CH-1015 Lausanne
Switzerland

Abstract. A fast spectroscopic system for superficial and local determination of the absorption and scattering properties of tissue (480 to 950 nm) is described. The probe can be used in the working channel of an endoscope. The scattering properties include the reduced scattering coefficient and a parameter of the phase function called γ, which depends on its first two moments. The inverse problem algorithm is based on the fit of absolute reflectance measurements to cubic B-spline functions derived from the interpolation of a set of Monte Carlo simulations. The algorithm's robustness was tested with simulations altered with various amounts of noise. The method was also assessed on tissue phantoms of known optical properties. Finally, clinical measurements performed endoscopically *in vivo* in the stomach of human subjects are presented. The absorption and scattering properties were found to be significantly different in the antrum and in the fundus and are correlated with histopathologic observations. The method and the instrument show promise for noninvasive tissue diagnostics of various epithelia. © *2003 Society of Photo-Optical Instrumentation Engineers.* [DOI: 10.1117/1.1578494]

1 Introduction

The optical properties of a biological tissue depend on its biochemical composition and its cellular and subcellular structure. Therefore optical measurements have a strong potential for the development of noninvasive *in vivo* medical diagnostic tools, often called ''optical biopsy.'' Such techniques should significantly improve the efficiency of biopsies or help in determining the tumor margins in a surgical field. Several types of optical properties can be measured, such as fluorescence,[1,2] Raman scattering,[3] and absorption and scattering,[2,4–8] each of them giving complementary information on the tissue.[4]

We focus in this paper on the absorption and scattering properties of tissue. In the visible and near-infrared range, the absorption spectrum is related to the concentration of chromophores, such as oxyhemoglobin and deoxyhemoglobin, fat and water.[9] Such chromophores vary significantly with tissue metabolism.[10] The scattering properties are related to the size distribution of cells and organelles, which are parameters used to differentiate normal from abnormal tissues in standard histopathology.[5,6] Previous studies showed that the absorption and scattering of tumor tissues differ from their surrounding normal tissue.[7,11,12]

The absorption and scattering properties of a bulk tissue can be calculated from measurements of the diffuse reflectance using an appropriate model of the light propagation in tissue. Such techniques have been extensively described when interrogating a relatively large part of the tissue, typically cubic centimeters.[10–12] In such cases, the light propagation can be modeled using diffusion theory.[13,14] Nevertheless, potential medical applications, such as biopsy guidance, require the investigation of a small volume of tissue, on the order of few cubic millimeters. In such a case, only small source–detector separations must be used.

Promising results have been obtained using spectroscopic reflectance measurements at a short source–detector separation,[2,4–7,15,16] demonstrating that important diagnostic information is contained in the reflectance spectrum. Nevertheless, most groups base their analysis on the wavelength dependence of the raw reflectance, without separating the absorption and scattering properties. In such a case, the interpretation of the reflectance spectrum in terms of tissue physiology is difficult, owing to coupling between the tissue absorption and scattering properties. Since absorption and scattering are fundamentally linked with different aspects of tissue physiology, and chromophore content and structure, respectively, the determination of both properties individually is expected to improve the discrimination among different tissues types and/or alterations.

We showed recently,[7,17] along with other groups,[4,8,18] that the local and superficial (average volume of 1 mm^3) determination of the scattering and absorption properties of tissue was possible noninvasively. Our method relies on the measurements of reflectance spectra at different small source–detector separations, and on a model based on Monte Carlo simulations. The model takes into account the influence of the phase function and does not require any assumption about the optical properties of the medium, unlike other methods.[4,8,18] Moreover, the use of spatially resolved reflectance could ac-
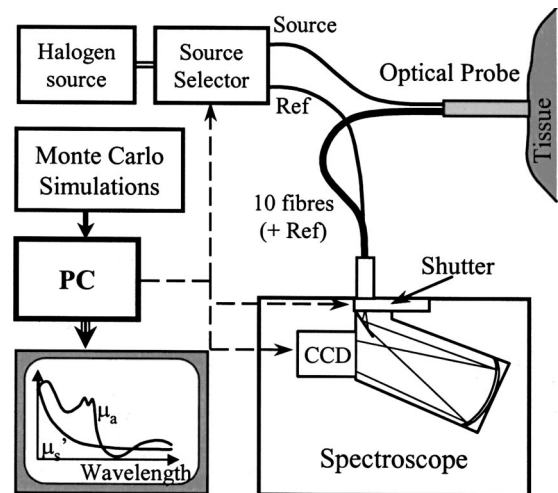

Fig. 1 General scheme of the acquisition setup.

commodate more complex models that take into account multilayer geometries.[19]

As shown recently by Kienle et al.,[20] the accuracy of the optical properties can be adversely affected if the effect of the phase function is not incorporated into the model. We consider the phase function parameter $\gamma = (1 - g_2)/(1 - g_1)$, where g_1 and g_2 are the first two moments of the phase function, respectively. This parameter is the most important parameter of the phase function for reflectance measurements close to the source,[17] and is related to the size distribution of scatterers inside the tissue.

In a previous paper we reported measurements performed *in vivo* on human brain.[7] The measurements were performed only at few wavelengths and the data processing was not optimized. We present here further experimental validation and several significant improvements of the method, which make it routinely applicable in clinical situations. In particular, we built an instrument and an optical probe capable of measuring spectrally and spatially resolved reflectance through the working channel of an endoscope. We also developed an efficient and fast algorithm for the determination of broadband spectra of the absorption coefficient, reduced scattering coefficient, and phase function parameter γ, based on cubic B-spline interpolation of Monte Carlo simulations.

We first describe the methodology, including the experimental setup and the fitting algorithm. Second, we report results on the accuracy and precision of the method, based on simulations and tissue phantoms of known optical properties. Third, we report *in vivo* clinical measurements performed endoscopically on a human gastrointestinal tract.

2 Materials and Methods

2.1 *Experimental Setup*

The schematic of the experimental setup is shown in Fig. 1. The light source is a halogen lamp (Ocean Optics LS-1) that is stabilized (variations less than 1% after 40 min of warming up). Other light sources can be selected by an optical switch. The optical switch has one output connected to the illuminating fiber of the optical probe and another one to a reference
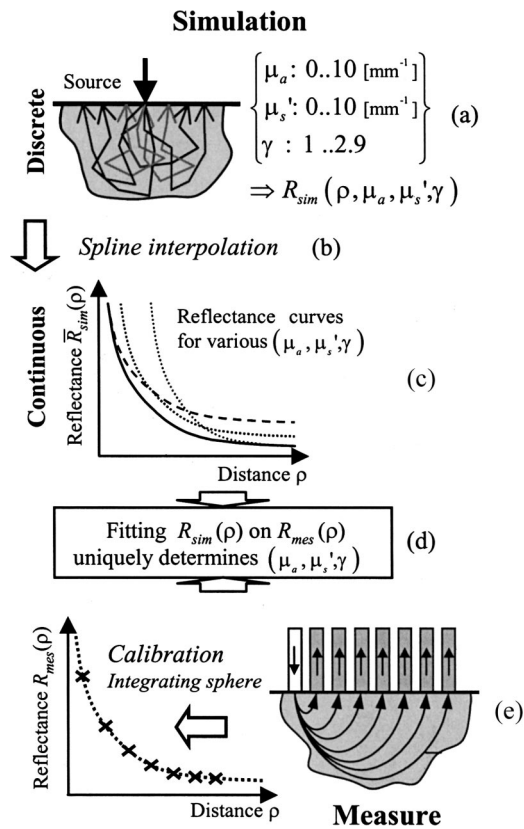
Simulation

Fig. 2 Diagram of the algorithm for the automatic spectral determination of μ_a, μ_s', and γ. (a) First, a set of reflectance curves simulated by the Monte Carlo method is produced for a wide range of discrete values for each optical coefficient (i.e., μ_a, μ_s', and γ). (b) Second, the simulated curves are interpolated by cubic B-splines to provide a reflectance curve (c) for any value of μ_a, μ_s', and γ. Finally, for each wavelength of the spectrum, a fit (d) of the measured reflectance curve (e) is performed onto the interpolated set of simulated curves, allowing for the determination of μ_a, μ_s', and γ. The fitting algorithm used is Levenberg-Marquardt.

channel that is connected directly to the spectrometer. Temporal variations of the source spectrum are corrected by the measurement made on the reference channel.

The optical probe is made of eleven optical fibers, one for illumination and ten for detection [see Fig. 2(e)]. The fibers usedare multimode silica fibers (FVP-200 PF from Thorlabs Inc.) with a numerical aperture of 0.22 and a core diameter of 200 μm. They are coated with a 20-μm polyimide sheath. The ten detection fibers are placed at various distances (noted as ρ_i, $i = 1$–10) from the illumination fiber, ranging approximately from 0.3 to 1.35 mm with a step of approximately 0.1 mm. They are held in place in the probe by two laser micromachined alignment pieces. This procedure leads to a high accuracy in fiber positioning (approximately 15 μm), which allows the construction of several identical probes. All the components have been chosen to with stand routine disinfections and/or sterilization without damage.

The ten detecting fibers are connected to an imaging spectrometer (Jobin-Yvon CP 200) with a Peltier-cooled CCD camera (Hamamatsu C7041 and S7031-1008). A mechanical shutter sets the integrating time of the CCD camera (usually about 600 ms). The image acquired on the camera is digitized

by a 12-bit analog/digital card (National Instrument PCI-MIO-16E-4). A single computer is used to control the instrumentation and to process the data. A typical measurement takes 4 s, including a first acquisition while the tissue is illuminated by the source fiber and a second acquisition made with the source fiber switched off. This allows the subtraction of the dark current noise and the background light.

In order to obtain absolute reflectance spectra, a two-step calibration procedure is performed. First, the effect of the spectral responses of the source, fibers, grating, and detector is corrected by performing a measurement on a spectrally flat reflectance standard. Typically, the probe is inserted inside an integrating sphere (made of Spectralon SRS-99, Labsphere Inc.). Second, the effective source intensity is obtained by performing a series of measurements on a solid turbid siloxane phantom whose optical properties (μ_a, μ_s', and γ) were previously determined at 675 nm by combining frequency-domain and spatially resolved measurements.[7] The comparison of the phantom measurement with the expected absolute reflectance from a Monte Carlo simulation allows the calibration of the absolute intensity of the experimental reflectance. Note that this calibration factor is wavelength independent, since all the spectral features of the instrumentation have been corrected in the first step. This calibration routine is performed every time the probe is reconnected to the setup, before or after the measurement session. Repeated measurements on the calibration phantom over a six-month period showed a standard deviation of approximately 4%, which was mostly due to the variability of the coupling between the probe and the phantom. Once the absolute reflectance spectra are calculated, the optical coefficients $\mu_a(\lambda)$, $\mu_s'(\lambda)$ and $\gamma(\lambda)$ are determined by the algorithm presented in Sec. 2.4.

2.2 Optical Model at Short Source–Detector Distances: The γ Parameter

Consider a tissue illuminated by a fiber with a unit of incident power. The spatially resolved reflectance $R(\rho)$ is defined as the power of the backscattered light per unit of area detected by a second fiber at the surface of the tissue at a distance ρ from the source. $R(\rho)$ depends on the optical properties of the sample, i.e., the absorption coefficient μ_a, the scattering coefficient μ_s, and the phase function $p(\cos \theta)$ (where θ is the scattering angle), the refractive index n, and the numerical aperture NA of the detecting fibers.

The phase function can be expanded into a series of Legendre polynomials $P_n(\cos \theta)$:

$$p(\cos \theta) = \sum_n (2n+1)g_n P_n(\cos \theta). \qquad (1)$$

In this expression, g_n is the n'th order moment of the phase function:

$$g_n = 2\pi \int_0^\pi P_n(\cos \theta)p(\cos \theta)d(\cos \theta), \qquad (2)$$

where g_1 is the conventional anisotropy factor, generally noted as g. In the diffusion approximation of the transport theory, g_1 is the only parameter used to describe the phase function. In this case, it is useful to define the reduced scattering coefficient $\mu_s' = \mu_s(1 - g_1)$.

The diffusion approximation generally holds for $\mu_s'\rho>5$ and $\mu_s'>100\mu_a$. For shorter source–detector separations, typically when $0.5<\mu_s'\rho<5$, we showed[17] that the second moment of the phase function g_2 must also be taken into account. This case corresponds to the measurement performed with the probe described in Sec. 2.1.

Using the similarity relations introduced by Wyman et al.,[21] it is easy to show that besides the refractive index, only three parameters are needed to accurately describe the light propagation at such short source–detection distances[17]: μ_a, μ_s', and γ where

$$\gamma = \frac{1-g_2}{1-g_1} \tag{3}$$

and γ depends on the scatterer's relative refractive index and on the ratio between the scatterer size and the wavelength; γ varies between 0.9 (Rayleigh-type scattering) and values larger than 2 (large scatterers compared with wavelength). We also showed that for a fractal distribution, γ is related to the fractal power of the size distribution of the scatterers.[22] Note also that for a Henyey-Greenstein phase function, $g_2 = g_1^2$ and, therefore,

$$g = g_1 = \gamma - 1. \tag{4}$$

2.3 Monte Carlo Simulation

We used Monte Carlo simulations as our basis for the model of light propagation. As already mentioned, standard diffusion theory is inadequate for the small source–detector separation we used in experiments[17] The Monte Carlo simulations allow us to generate reflectance curves noted as $R_{\text{sim}}(\rho_i,\mu_a,\mu_s',\gamma)$ [see Fig. 2(a)]. The code we used has been extensively tested and allows the use of any phase function given in discretized form,[23,24] We used a modified form of the Henyey-Greenstein[25] phase function $p_{\text{HG}}(\theta,g_{\text{HG}})$, noted as $p_{\text{MHG}}(\theta,g_{\text{HG}},\xi)$ (see Ref. 17):

$$p_{\text{MHG}}(\theta,g_{\text{HG}},\xi) = \xi \times p_{\text{HG}}(\theta,g_{\text{HG}}) + (1-\xi)\frac{3}{4\pi}\cos^2\theta$$

$$\xi = 0-1, \tag{5}$$

where ξ is a normalization factor. According to Eq. (1), adding the $\cos^2\theta$ term only affects the value of g_2. Thus, choosing g_1 and g_2, i.e., setting γ, uniquely determines the values of g_{HG} and ξ. The tissue was considered to be homogeneous and its refractive index was fixed at 1.4. Our simulations took into account the geometry of the probe. The fibers had a diameter of 200 μm; the index mismatch between the probe ($n=1.5$) and the tissue was taken into account by the Fresnel law. We showed in a previous paper[7] that for the type of probe used in the experiment, the index mismatch outside the probe does not play a significant role.

In order to decrease the Monte Carlo noise and limit the number of photons (one million photons have been simulated for each reflectance curve), the numerical aperture was set at a higher value than in the experiments (0.279 instead of 0.157). This use of the higher numerical aperture was chosen as a tradeoff between simulation time, noise in the simulation, and accuracy degradation. Several tests showed that after

renormalization of the intensity, this mismatch introduced a typical error smaller than 2% and a maximum error of 4%. Note that in both the simulation and the experiments, the numerical aperture corresponds to a narrow solid angle (a half angle of 16° instead of 9°) and the angular distribution is close to a Lambertian distribution for such small-angle ranges.

Approximately forty discrete values were chosen for μ_a and μ_s', ranging respectively from 0.003 to 10 mm^{-1} and from 0.5 to 10 mm^{-1}; twenty values were chosen for γ, ranging from 1.0 to 2.9. This resulted in a four-dimensional matrix of simulated reflectance curves, noted as $R_{\text{sim}}(\rho_i,\mu_a,\mu_s',\gamma)$, each coefficient taking only discrete values. Using these parameters, 32,000 reflectance curves have been computed, each for a specific triplet of optical coefficients (μ_a,μ_s',γ). Since the path lengths and exit positions of each simulated photon were stored, a full Monte Carlo simulation was required only for each different value of γ (thus twenty simulations only). Assuming the tissue is homogeneous, scaling relationships[17] allow us to derive any reflectance curve $R_{\text{sim}}(\rho_i,\mu_a,\mu_s',\gamma)$ from a single simulation $R_{\text{sim}}(\rho_i,\mu_a=0,\mu_s'=1,\gamma)$, γ being kept constant.

2.4 Algorithm for the Determination of μ_a, μ_s', and γ

We denote ρ_i, $i=1-10$, the distances between the ten detecting fibers and the illuminating fiber, and $R_{\text{mes}}(\rho_i)$ as the measured reflectance at these distances for a given wavelength. The inverse problem corresponds to determining the optical coefficient triplet (μ_a,μ_s',γ) that is the closest to the reflectance curve $R_{\text{mes}}(\rho_i)$.

The basic idea of the algorithm, as shown in Fig. 2, is to fit the measured reflectance curve $R_{\text{mes}}(\rho_i)$ onto a set of previously simulated reflectance curves, forming a matrix noted as $R_{\text{sim}}(\rho_i,\mu_a,\mu_s',\gamma)$. An algorithm based on a lookup table can be performed as a first step. However, in such a case, the number of simulations performed naturally limits the accuracy of the result. Since the reflectance curves are continuous in all their parameters, this problem could be overcome by interpolating the basic set of simulations. The result of the interpolation is thus a function $\bar{R}_{\text{sim}}(\rho_i,\mu_a,\mu_s',\gamma)$, which is a numerical function defined for any value of the optical coefficient triplets (μ_a,μ_s',γ) within their definition ranges and for each discrete distance ρ_i, $i=1-10$.

The matrix $R_{\text{sim}}(\rho_i,\mu_a,\mu_s',\gamma)$ was interpolated with cubic B-splines.[26] Schönberg et al.[27] have shown that any discrete function $R(x)$, $(x \in \mathbb{Z})$ may be interpolated by a unique combination $c(k)$ of B-splines $\beta^n(x)$:

$$R(x) = \sum_{k \in Z} c(k)\beta^n(x-k), \tag{6}$$

where $c(k)$ is the weighing coefficient of the B-spline $\beta^n(x-k)$ centered on k.

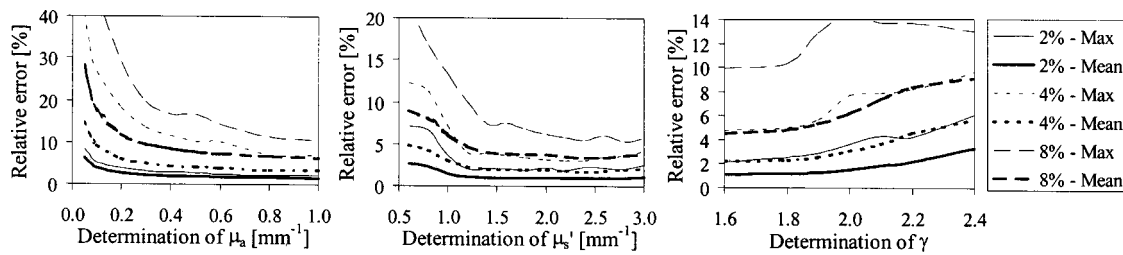Cubic B-splines $\beta^3(x)$ are defined like pieces of polynomials of degree 3, smoothly connected:

Fig. 3 Accuracy of the algorithm to determine μ_a, μ_s', and γ from noisy reflectance curves. The relative amplitudes of uniformly distributed noise added to the simulated reflectance curves were 2, 4, and 8%, and both the maximal (thin lines) and average (bold lines) inaccuracies are plotted.

$$\beta^3(x) = \begin{cases} \frac{2}{3} - |x|^2 + |x|^3/2 & |x| \leq 1 \\ (2 - |x|)^3/6 & 1 < |x| \leq 2 \\ 0 & |x| > 2 \end{cases} \qquad (7)$$

Interpolation of multivariable functions is generalized by replacing $c(k)$ by $c(k,l,...,m)$ and by replacing $\beta^n(x-k)$ by $\beta^n(x-k) \times \beta^n(y-l)...\beta^n(z-m)$ in Eq. (6), the number of B-splines matching the number of variables. The derivative of the function $R(x)$ may also easily be obtained by replacing the B-spline function by a combination of B-splines of the inferior degree but keeping the same coefficients $c(k)$.

If the function $R(x)$ is known on x values that are not integers—as is the case for the reflectance matrix $R_{\text{sim}}(\rho_i, \mu_a, \mu_s', \gamma)$—it must be made uniform. This step is performed by interpolating the function with nonuniform splines, resampling it on the integers, and finally interpolating it again with uniform B-splines. This process, fully described in Ref. 28, has been applied on $R_{\text{sim}}(\rho_i, \mu_a, \mu_s', \gamma)$.

In terms of performance, this interpolation method is very efficient because the initial matrix $R_{\text{sim}}(\rho_i, \mu_a, \mu_s', \gamma)$ is economically replaced by a matrix of coefficients $c(\rho_i, k, l, m)$ of the same dimension, and any value of $\bar{R}_{\text{sim}}(\rho_i, \mu_a, \mu_s', \gamma)$ is calculated by the summation of 3×4 B-splines weighted by their coefficients $c(\rho_i, k, l, m)$.* The interpolated function $\bar{R}_{\text{sim}}(\rho_i, \mu_a, \mu_s', \gamma)$ could then be properly used to fit any measured reflectance curve in order to determine its optical coefficients. To perform the fit, the Levenberg-Marquardt algorithm was chosen because of its efficiency and its robustness. Appropriately, this algorithm minimizes the quantity noted as χ^2 and defined as

$$\chi^2 = \sum_{i=1}^{10} \left(\frac{R_{\text{mes}}(\rho_i) - \bar{R}_{\text{sim}}(\rho_i, \mu_a, \mu_s', \gamma)}{\sigma_i} \right)^2, \qquad (8)$$

where σ_i is the standard deviation of each data point.

As required by the algorithm, the Jacobean of the $\bar{R}_{\text{sim}}(\rho_i, \mu_a, \mu_s', \gamma)$ function can be calculated economically, as mentioned before, by the combination of square B-splines. For the lowest wavelength, a first set of parameters (μ_a, μ_s', γ) is determined using a lookup table based on the discrete set of simulations $R_{\text{sim}}(\rho_i, \mu_a, \mu_s', \gamma)$. These values

are then used as initial guesses for the Levenberg-Marquardt algorithm. For the next wavelength, the initial values are taken directly from the previous wavelengths (typically from an average of the four closest wavelengths). Nevertheless, we found the converged values to be insensitive to the initial guesses, which is related to the fact that only single minima were found in the χ^2 function, as discussed in the next section. The determination of the optical coefficients for a whole spectrum, composed of 510 wavelengths (480 to 950 nm) takes about 50 s (on a 400-MHz Pentium personal computer).

3 Results and Discussion

3.1 Algorithm Robustness to Noise

Various assessments of the algorithm are reported in this section. First, in order for the algorithm to work properly, its solution must be unique. This is guaranteed if only a single minimum is present in the χ^2 function. An inspection of the χ^2 function over the whole range of values of μ_a, μ_s', and γ for which the algorithm is defined (i.e., μ_a from 0.003 to 10 mm^{-1}, μ_s' from 0.5 to 10 mm^{-1}, and γ from 1.0 to 2.9) revealed only a single minimum for each set of parameters. Second, the robustness of the algorithm was studied by assessing the impact of noise on the accuracy of the optical coefficient determination. For this, noise (uniformly distributed) was added to simulated experimental reflectance curves. The relative errors between the result of the fit and the expected optical properties were estimated and are shown in Fig. 3 for noise of 2, 4, and 8% of the reflectance curve. Such noise figures are realistic for clinical tissue measurements, where tissue heterogeneity plays a significant role as noise in the reflectance curve. For each noise value, both the maximal and average errors of determination are plotted. Typically, the mean error on μ_s' and γ is lower than 3, 5, and 10% for a noise of 2, 4, and 8%, respectively. The maximum error on μ_a is lower than 6, 15, and 30% for a noise of 2, 4, and 8%, respectively. The determination of μ_a is the most sensitive to noise because the sensitivity of the measurement to the absorption is not optimal owing to the relatively short path length at a short source–detector separation. Also, the error increases significantly at low absorption, especially for absorptions lower than 0.05 mm^{-1}. Specifically, μ_a values smaller than 0.02 mm^{-1} cannot be reasonably estimated accurately with such a small source–detector separation. Therefore this method is best adapted to wavelengths in the visible (400 to 700 nm) or wavelengths higher than 900 nm, where μ_a is typically higher than 0.02 mm^{-1} in tissues. Overall,

---

*Since there are three variables, μ_a, μ_s' and γ, the expression of $R_{\text{sim}}(\rho_i, \mu_a, \mu_s', \gamma)$ requires three B-splines. But then the infinite summation on $k \in \mathbb{Z}$ may be reduced to four terms because the splines are all zero outside the interval $]-2;2[$.
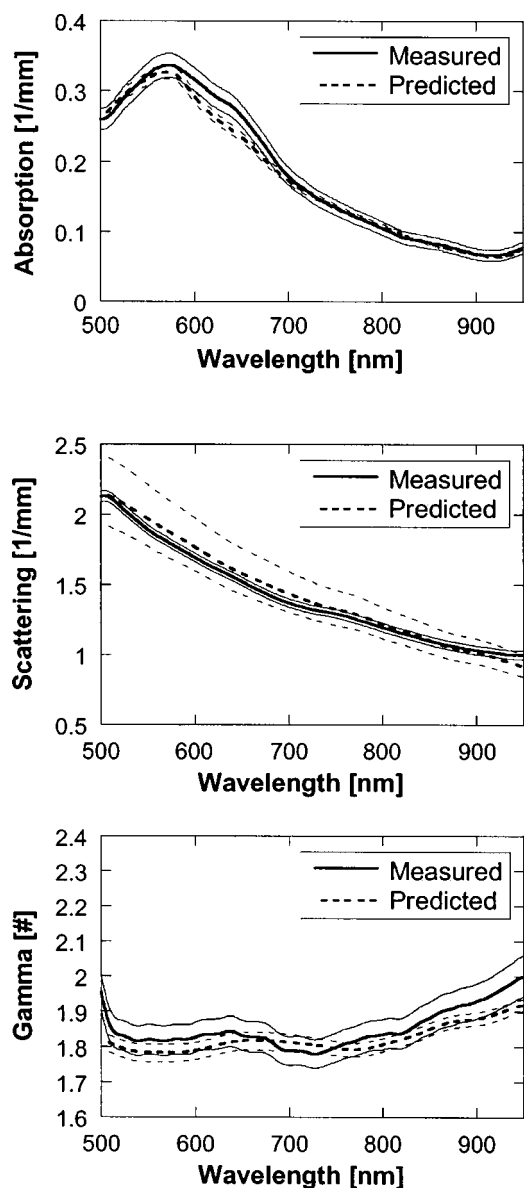
Fig. 4 Comparison of the predicted spectra of optical coefficients (dashed curve) and those measured (solid curve) on the phantoms. The bold line is the average and the thin solid ones are the standard deviations.

these results demonstrate that μ_a, μ_s', and γ can be determined simultaneously from the reflectance curve at short source–detector separations, which is a remarkable result.

3.2 Experiments With Phantoms

In order to complete the validation of the method, we performed a series of measurements on tissuelike phantoms made of suspended and dyed microspheres. Gélébart et al.[29] have suggested that tissue phase functions could be advantageously simulated with a mixture of spheres with different diameters. Following this approach, we mixed polystyrene microspheres of five different diameters: 1, 0.5, 0.2, 0.1, and 0.05 μm. An identical concentration of 1.3 [g/liter] was set for each diameter, corresponding to a sphere density decreasing as d^{-3}, where d is the sphere's diameter. The scattering spectra $\mu_s'(\lambda)$

and $\gamma(\lambda)$ were calculated by Mie theory,[30] assuming a refractive index of 1.60 for polystyrene and 1.33 for water.

The absorption properties of the solution were obtained by adding Nigrosin to the microsphere suspensions with a concentration of 59.09 ± 1.65 μg/ml. The Nigrosin absorption spectrum $\mu_a(\lambda)$ was determined by spectrophotometry. Figure 4 shows a comparison of the predicted spectra of optical coefficients $\mu_a(\lambda)$, $\mu_s'(\lambda)$, and $\gamma(\lambda)$ and the corresponding spectra measured experimentally with the probe.

A preliminary analysis allowed us to make two adjustments in the experimental procedure that eliminated two sources of systematic errors. First, we found that the use of the two closest fibers ($\rho \approx 0.3$) did not fit well with the simulations and was causing a systematic error. This effect was most likely due to a mismatch in higher moments of the phase function between our theoretical and experimental models. Our theoretical model assumes that only the first two moments of the phase function affect the reflectance. We showed in Ref. 17 that such an assumption is valid for an optical distance $\rho \mu_s' > 0.5$. Shorter distances can be used only if higher moments are matched between the simulation and experiment. This is indeed generally not the case between the average phase function of microsphere mixtures made of only five sizes of spheres and the modified Henyey-Greenstein phase function used in the simulation. Thus, these two fibers were removed from the analysis of the phantom measurements. However, the first two fibers have been kept when analyzing tissue measurements, since in this case the high-order moments of the tissue phase function are expected to match significantly better with the ones of the modified Henyey-Greenstein phase function. Moreover, adding these two fibers improved the robustness of the fit. Second, a systematic difference of 5% was found in the reflectance intensity between experiments and simulations, which was mainly due to the refractive index difference between the phantom ($n = 1.33$) and the refractive index assumed in the simulations ($n = 1.40$, corresponding to tissue).

Figure 4 shows the comparison between the predicted and experimental $\mu_a(\lambda)$, $\mu_s'(\lambda)$, and $\gamma(\lambda)$ values. The agreement on $\mu_s'(\lambda)$ and $\gamma(\lambda)$ is excellent, with an error typically less than 5%. A good agreement is also found for $\mu_a(\lambda)$ with an error less than 10%. These results confirmed the algorithm test described in the previous section.

3.3 In Vivo Measurements of Human Gastrointestinal Tracts

In this section we present measurements performed in vivo on the human stomach, in the antrum (lower part of the stomach) and fundus (upper part) during gastroscopic examination. These results represent an example of the clinical feasibility of the method. Other studies are currently being performed on the colon and the uterus. One of the medical interests of the method lies in the possibility of instantly discriminating gastritis from normal cases in vivo during gastroscopy. This necessitates the determination of normal values for the mucosa in the antrum and in the fundus, which are presented here. In a companion paper,[31] we will report further studies on the stomach, showing that this technique is sensitive to different stages of gastritis and to subtypes as well.[32]
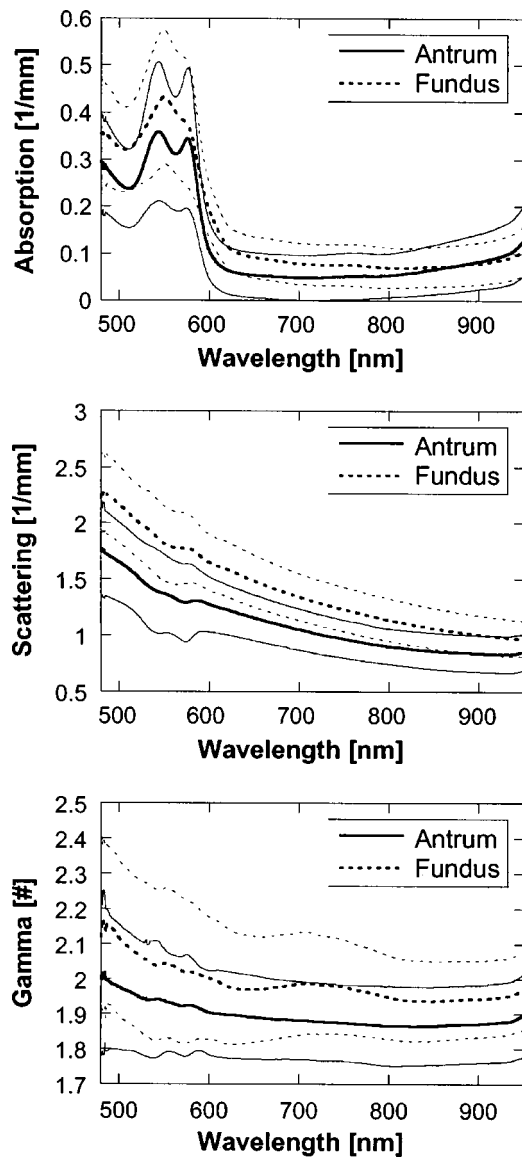
(a) Antrum   **(b) Fundus**

Fig. 6 Histological slices of antrum (a) and fundus (b). Whereas the layered structure is clearly visible in the fundus with the glandular region (G) clearly distinct from the foveolar (F), the structure of the epithelium is thinner and less contrasted in the antrum. Moreover, the mucosa is two times thicker in the fundus than in the antrum.

Fig. 5 Average (bold lines) and standard deviations (thin lines) of optical coefficients measured for normal antrum (solid curve) and normal fundus (dashed curve).

A set of 35 patients, 21 females and 14 males, aged from 23 to 87 with an average age of 50 were examined. For each patient, four sites were usually selected to be measured, two in the antrum and two in the fundus. The optical probe was inserted into the working channel of the gastroscope at the end of the examination and gently applied on the tissue. The pressure could not be monitored during acquisition, but other controlled measurements on mouse skin showed that pressure variations did not significantly alter the results.

The endoscope illumination was turned off after the probe placement because of its high intensity. During this time, four to six measurements were taken in approximately 20 s. At the end, the endoscope illumination was turned on again and measurements were accepted and averaged if the probe stayed at the same location. The accept rate was approximately 80%. Immediately after that, a biopsy was taken on the measurement site, which could be precisely located by a light mark on the epithelium. The data were analyzed after the clinical session.
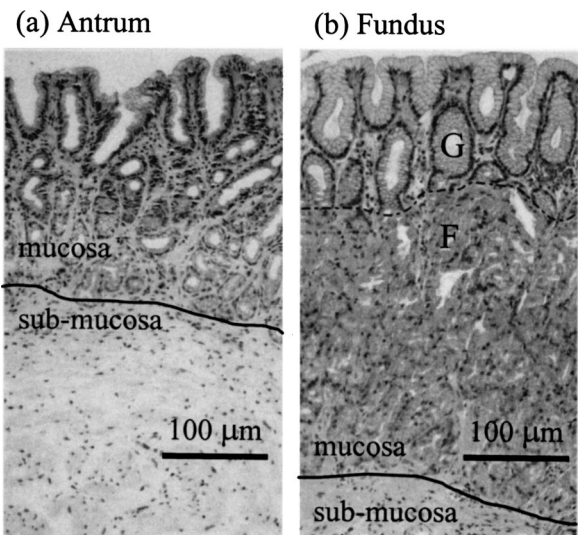
Figure 5 shows the average optical properties, $\mu_a(\lambda)$, $\mu_s'(\lambda)$, and $\gamma(\lambda)$, of twenty-two measurements performed in the antrum and sixty measurements performed in the fundus. All sites were found normal after biopsy. First, as expected, $\mu_a(\lambda)$ clearly shows the presence of hemoglobin, characterized by absorption peaks at 541 and 576 nm. The absorption decreases significantly in the near-infrared range. The slight increase for wavelengths larger than 850 nm is due to water and hemoglobin. The concentration of total oxyhemoglobin (HbO_2) and deoxyhemoglobin (Hb) were obtained by a least-square fit of $\mu_a(\lambda)$. The total hemoglobin concentration (i.e., $[HbO_2]+[Hb]$) was 20.0 ± 2.6 μM in the antrum, with a saturation (sO_2) around 48%. In the fundus, a similar total hemoglobin concentration was found, 21.0 ± 2.6 μM, whereas the saturation drops to 21%. This surprising very low saturation could nevertheless be explained by a high concentration of CO_2 in the mucosa. Further investigations are needed to validate such results, since no other data on the oxygenation and saturation of hemoglobin in the fundus mucosa have been published yet. The $\mu_s'(\lambda)$ spectra measured in both the fundus and antrum are monotonically decreasing, corresponding approximately to a power function, as expected for tissue.[9,29,33] The scattering spectrum $\mu_s'(\lambda)$ is found to be significantly lower in the antrum than in the fundus over nearly the entire spectrum.

The $\gamma(\lambda)$ spectra are approximately constant. This is consistent in the case of a large distribution of scatterer sizes, as found in tissue. As a matter of fact, similar findings were displayed in the experiment and simulation using the microsphere suspensions. Computations with Mie scatterers showed that the $\gamma(\lambda)$ value is related to the scatterer size distribution.[22,32] Therefore the absolute γ value might be important in differentiating tissue types.

For the antrum and the fundus, the γ values are 1.9 ± 0.1 and 2.0 ± 0.1, respectively. Assuming a Henyey-Greenstein phase function, these values would correspond to a g of 0.9 and higher. Such values are basically in agreement with g values commonly accepted for tissue. However, the γ values are found in some cases to be larger than 2, which could not be produced by a simple Henyey-Greenstein phase function. This seems to confirm previous results showing that a Henyey-Greenstein function alone does not approximate the tissue phase function adequately at large angles, but needs to be completed by either a second Henyey-Greenstein function with a negative g value or a $\cos^2 \theta$ function.[17,20]

The differences between the fundus and antrum found in the scattering properties $\mu_s'(\lambda)$ and $\gamma(\lambda)$ can be correlated with the histological analysis of the biopsy samples. Figure 6 shows typical histological images of tissue resected after measurements. These images clearly show a difference in the thickness of the foveolar and glandular regions between the antrum and the fundus. These differences are likely to be the source of the differences observed in the $\mu_s'(\lambda)$ and $\gamma(\lambda)$ coefficients. We recently showed[34] correlations between spectra of optical coefficients measured with this setup and histological analysis of a mouse skin alteration model.

Globally, these results demonstrate that the scattering, $\mu_s'(\lambda)$ and $\gamma(\lambda)$, and absorption, $\mu_a(\lambda)$, properties of the tissue can be separated quantitatively. Only a fairly small coupling effect with the $\mu_a(\lambda)$ spectrum can be observed in both $\mu_s'(\lambda)$ and $\gamma(\lambda)$ spectra. Such a coupling is unavoidable considering that actual tissue is not homogeneous, which is the opposite of the theoretical model. As already mentioned, the layer structure is obvious in Fig. 6.

Two approaches are possible to further diminish such a coupling and improve accuracy. First, the $\mu_a(\lambda)$, $\mu_s'(\lambda)$, and $\gamma(\lambda)$ spectral shapes could be constrained. The $\mu_a(\lambda)$ spectrum can be assumed to result from known chromophores such as Hb, HbO_2, water and fat. As discussed earlier, in tissue, $\mu_s'(\lambda)$ approximately follows a power law and $\gamma(\lambda)$ is approximately a linear function. Incorporating such conditions in the inverse problem would significantly decrease coupling effects. Second, a layer model could be used to more closely model the tissue structure. Spatially resolved measurements seem appropriate to determine some of the properties of a two-layer geometry.[19]

4 Conclusions

We have presented a method to determine the scattering and absorption spectra of small volumes of tissue *in vivo*. This method is based on the measurement of the spatially and spectrally resolved reflectance with a small optical probe (2.3-mm diameter), that can be used in the working channel of endoscopes. Three coefficients are determined simultaneously from the measurements, $\mu_a(\lambda)$, $\mu_s'(\lambda)$, and the phase function parameter $\gamma(\lambda)$. The computation of these parameters was obtained from a Levenberg-Marquardt fit of the measured reflectance to cubic B-spline interpolation of Monte Carlo simulations.

The robustness of the algorithm has been assessed using simulated reflectance curves, adding various degrees of noise. These results showed that $\mu_a(\lambda)$ is the coefficient most sensitive to noise, especially for low absorption. The accuracy of

the method was also tested on tissue phantoms with known optical properties. A good agreement between the measurement and prediction was found. Typically, $\mu_a(\lambda)$, $\mu_s'(\lambda)$, and $\gamma(\lambda)$ can be determined with an error smaller than 10%.

The ability to perform clinical measurements was demonstrated. Measurements on 35 patients were performed on the stomach epithelium through the working channel of a gastroscope. The average was found to be significantly different in the antrum and in the fundus. To our knowledge, these measurements are the first report of the simultaneous *in vivo* determination of broadband spectra of the absorption coefficient $\mu_a(\lambda)$, reduced scattering coefficient $\mu_s'(\lambda)$, and phase function parameter $\gamma(\lambda)$. We believe that this method has promise for providing important clinical information to guide biopsies efficiently.

References

1. N. Ramanujam, "Fluorescence spectroscopy of neoplastic and non-neoplastic tissues," *Neoplasia* **2**, 89–117 (2000).
2. I. Bigio and J. R. Mourant, "Ultraviolet and visible spectroscopies for tissue diagnostics: Fluorescence spectroscopy and elastic-scattering spectroscopy," *Phys. Med. Biol.* **42**, 803–814 (1997).
3. A. Mahadevan-Jansen and R. Richards-Kortum, "Raman spectroscopy for the detection of cancers and precancers," *J. Biomed. Opt.* **1**, 31–70 (1996).
4. I. Georgakoudi, B. C. Jacobson, J. Van Dam, V. Backman, M. B. Wallace, M. G. Müller, Q. Zhang, K. Badizadegan, D. Sun, G. A. Thomas, L. T. Perelman, and M. S. Feld, "Fluorescence, reflectance, and light-scattering spectroscopy for evaluating dysplasia in patients with Barrett's esophagus," *Gastroenterology* **120**, 1620–1629 (2001).
5. L. T. Perelman, V. Backman, M. Wallace, G. Zonios, R. Manoharan, A. Nuserat, S. Shields, M. Seiler, C. Lima, T. Hamano, I. Itzkan, J. Van Dam, J. M. Crawford, and M. S. Feld, "Observation of periodic fine structure in reflectance from biological tissue: a new technique for measuring nuclear size distribution," *Phys. Rev. Lett.* **80**(3), 627–630 (1998).
6. V. Backman, M. B. Wallace, L. T. Perelman, J. T. Arendt, R. Gurjar, M. G. Müller, Q. Zhang, G. Zonios, E. Kline, T. McGillican, S. Shapshay, T. Valdez, K. Badizadegan, J. M. Crawford, M. Fitzmaurice, S. Kabani, H. S. Levin, M. Seiler, R. R. Dasari, I. Itzkan, J. Van Dam, and M. S. Feld, "Detection of preinvasive cancer cells," *Nature (London)* **406**(6791), 35–62 (2000).
7. F. Bevilacqua, D. Piguet, P. Marquet, J. D. Gross, B. J. Tromberg, and C. Depeursinge, "*In vivo* local determination of tissue optical properties: applications to human brain," *Appl. Opt.* **38**(22), 4939–4950 (1999).
8. G. Zonios, L. T. Perelman, V. Backman, R. Manoharan, M. Fitzmaurice, J. Van Dam, and M. S. Feld, "Diffuse reflectance spectroscopy of human adenomatous colon polyps *in vivo*," *Appl. Opt.* **38**, 6628–6637 (1999).
9. F. Bevilacqua, A. J. Berger, A. E. Cerussi, D. Jakubowski, and B. J. Tromberg, "Broadband absorption spectroscopy in turbid media by combining frequency-domain and steady-state methods," *Appl. Opt.* **39**, 6498–6507 (2000).
10. A. E. Cerussi, A. J. Berger, F. Bevilacqua, N. Shah, D. Jakubowski, J.

Butler, R. F. Holcombe, and B. J. Tromberg, "Sources of contrast for quantitative non-invasive optical spectroscopy of breast tissue physiology," *Acad. Radiol.* **8**, 211–218 (2001).

11. J. B. Fishkin, O. Coquoz, and B. J. Tromberg, "Frequency-domain photon migration measurements of normal and malignant tissue optical properties in a human subject," *Appl. Opt.* **36**(1), 10–20 (1997).

12. B. J. Tromberg, O. Coquoz, J. B. Fishkin, T. Pham, E. R. Anderson, J. Butler, M. Cahn, J. D. Gross, V. Venugopalan, and D. Pham, "Non-invasive measurements of breast tissue optical properties using frequency-domain photon migration," *Philos. Trans. R. Soc. London, Ser. B* **352**, 661–668 (1997).

13. A. Ishimaru, "Diffusion of a pulse in densely distrubuted scatterers," *J. Opt. Soc. Am.* **68**, 1045 (1978).

14. R. A. J. Groenhuis, J. J. Ten Bosch, and H. A. Ferwerda, "Scattering and absorption of turbid materials determined from reflection measurements. 2. Measuring method and calibration," *Appl. Opt.* **22**, 2463–2467 (1983).

15. R. Marchesini, N. Cascinelli, D. R. Ventrali et al., "*In vivo* spectrophotometric evaluation of neoplastic and non-neoplastic skin pigmented lesions. II: Discriminant analysis between nevus and melanoma," *Photochem. Photobiol.* **55**, 515–522 (1992).

16. V. P. Wallace, D. C. Crawford, and J. C. Bamber, "Spectrophotometric assessment of pigmented skin lesions: methods and feature selection for evaluation of diagnostic performance," *Phys. Med. Biol.* **45**, 735–751 (2000).

17. F. Bevilacqua and C. Depeursinge, "Monte Carlo study of diffuse reflectance at source–detector separations close to one transport mean free path," *J. Opt. Soc. Am. A* **16**(12), 2935–2945 (1999).

18. J. R. Mourant, I. J. Bigio, D. A. Jack, T. M. Johnson, and H. D. Miller, "Measuring absorption coefficients in small volumes of highly scattering media: source–detector separations for which path lengths do not depend on scattering properties," *Appl. Opt.* **36**, 5655–5761 (1997).

19. C. K. Hayakawa, J. Spanier, F. Bevilacqua, A. K. Dunn, J. S. You, B. J. Tromberg, and V. Venugopalan, "Perturbation Monte Carlo methods to solve inverse photon migration problems in heterogeneous tissues," *Opt. Lett.* **26**, 1335–1337 (2001).

20. A. Kienle, F. K. Forster, and R. Hibst, "Influence of the phase function on determination of the optical properties of biological tissue by spatially resolved reflectance," *Opt. Lett.* **26**, 1571–1573 (2001).

21. D. R. Wyman, M. S. Patterson, and B. C. Wilson, "Similarity relations for anisotropic scattering in Monte Carlo simulation of deeply penetrating neutral particles," *J. Comput. Phys.* **81**, 137–150 (1989).

22. P. Thueler, F. Bevilacqua, and C. Depeursinge, "Relationship between the phase function parameter γ and the dimension of a fractal distribution of scatterers," (submitted).

23. P. Marquet, F. Bevilacqua, C. Depeursinge, and E. B. de Haller, "Determination of the reduced scattering and absorption coefficient by a single charge-coupled-device array measurement. Part I: Comparison between experiments and simulations," *Opt. Eng.* **34**, 2055–2063 (1995).

24. F. Bevilacqua, "Local optical characterization of biological tissues *in vitro* and *in vivo*," PhD Thesis No. 1789, Swiss Federal Institute of Technology, Lausanne (1998).

25. L. G. Henyey and J. L. Greenstein, "Diffuse radiation of the galaxy," *Astrophys. J.* **93**, 70–83 (1941).

26. M. Unser, "Splines: A perfect fit for signal and image processing," *IEEE Signal Process. Mag.* **16**(6), 22–38 (1999).

27. I. J. Schönberg, "Contribution to the problem of approximation of equidistant data by analytic functions," *Quart. Appl. Math.* **4**, 45–99 and 112–141 (1946).

28. A. Muñoz Barrutia, T. Blu, and M. Unser, "Non-uniform to uniform grid conversion using least-squares splines," *Proceedings of the Tenth European Signal Processing Conference (EUSIPCO'00)*, Tampere, Finland, September 4–8, 2000, Vol. IV, pp. 1997–2000.

29. B. Gélébart, E. Tinet, J. M. Tualle, and S. Avrillier, "Phase function simulation in tissue phantoms: A fractal approach," *Pure Appl. Opt.* **5**, 377–388 (1996).

30. C. F. Bohren and D. R. Huffman, *Absorption and Scattering of Light by Small Particles*, Wiley, New York (1983).

31. I. Charvet, P. Thueler, G. Ory, M.-A. Brundler, M. Saint-Ghislain, A. Hadengue, C. Depeursinge, P. Meda, and B. Vermeulen, "Noninvasive diagnosis of gastritis alterations," (submitted).

32. P. Thueler, "Optical spectral probing for epithelial tissue characterization," PhD, Dissertation No. 2241, Swiss Federal Institute of Technology, Lausanne (2001).

33. J. R. Mourant, J. P. Freyer, A. H. Hielscher, A. A. Eick, D. Shen, and T. M. Johnson, "Mechanisms of light scattering from biological cells relevant to non-invasive optical tissue diagnostics," *Appl. Opt.* **37**(16), 3586–3593 (1998).

34. I. Charvet, P. Thueler, B. Vermeulen, M. Saint-Ghislain, C. Biton, J. Jacquet, F. Bevilacqua, C. Depeursinge, and P. Meda, "A new optical method for the noninvasive detection of minimal tissue alterations," *Phys. Med. Biol.* **47**, 2095–2108 (2002).